Superferromagnetism in mechanically alloyed fcc $Fe_{23}Cu_{77}$ with bimodal cluster size distribution

2009 J. Phys.: Condens. Matter 21 046003

(http://iopscience.iop.org/0953-8984/21/4/046003)

J. Phys.: Condens. Matter **21** (2009) 046003 (9pp) doi:10.1088/0953-8984/21/4/046003

Superferromagnetism in mechanically alloyed fcc $Fe_{23}Cu_{77}$ with bimodal cluster size distribution

N J O Silva[1,4], J S Amaral[1], V S Amaral[1], B F O Costa[2] and G Le Caër[3]

[1] Departamento de Física and CICECO, Universidade de Aveiro, 3810-193 Aveiro, Portugal
[2] CEMDRX, Physics Department, University of Coimbra, P-3004-516 Coimbra, Portugal
[3] Institut de Physique de Rennes, UMR UR1-CNRS 6251, Université de Rennes I, Campus de Beaulieu, Batiment 11A, F-35042 Rennes Cedex, France

E-mail: jamaral@ua.pt

Received 10 October 2008, in final form 25 November 2008
Published 22 December 2008
Online at stacks.iop.org/JPhysCM/21/046003

Abstract

Magnetic measurements, x-ray diffraction and Mössbauer spectroscopy were used to characterize a nanostructured fcc $Fe_{23}Cu_{77}$ at.% alloy prepared by high-energy ball-milling, addressing in particular the effect of clustering on the nature of the interacting magnetic entities. The interpretation of magnetization measurements leads to the conclusion that grains, whose mean size is ∼16 nm, contain two populations of magnetic Fe-rich nanoclusters with a bimodal size distribution. These two sets of clusters contain about 14 and 400 Fe atoms and have magnetic moments of 30 μ_B and 860 μ_B, respectively. The inter-cluster ferromagnetic interactions that lead to superferromagnetism with a Curie temperature $T_C \sim 220$ K can be described by a mean field determined by the smaller clusters only, which account for 90% of the magnetization.

(Some figures in this article are in colour only in the electronic version)

1. Introduction

Non-equilibrium synthesis processes are now in common use to produce a variety of metastable materials, e.g. amorphous alloys, extended solid solutions, out-of-equilibrium crystalline phases and nanostructured materials, with enhanced mechanical and physical properties suitable for high-performance materials. Alloys formed between constituents that show little or no mutual solubility in equilibrium conditions are of particular technological and scientific importance [1]. The mechanisms of intermixing of elements, the stability of such alloys and their phase transformations have been notably investigated [1–4]. Their morphologies with eventual nanoscale decomposition features may result in interesting physical properties, in particular magnetic properties. For instance, Co–Cu and Fe–Cu alloys have attracted particular attention since the discovery of the giant magnetoresistance effect for different iron concentrations [5, 6].

[4] Present address: ICMA, Departamento de Fisica de la Materia Condensada, Facultad de Ciencias, Zaragoza, Spain.

The binary Fe–Cu system is one of the most extensively studied among the many systems with positive heats of mixing. Iron and copper are essentially immiscible at room temperature and the equilibrium solubility of Cu in Fe remains as low as 0.14 at.% and 0.61 at.% at 723 K and 923 K, respectively [7]. Fe–Cu alloys have been synthesized by techniques like sputtering [8–11] and, since the 1990s, by mechanical alloying [12–42]. High-energy ball-milling of Fe and Cu powder mixtures with a starting composition Fe_xCu_{100-x} (at.%) induces the formation of nanostructured solid solutions, either bcc for Fe-rich Fe(Cu) alloys ($x \geqslant 80$) or fcc for Cu-rich ($x \leqslant$ 40–50) Cu(Fe) alloys while two phases (bcc + fcc) coexist in the intermediate range, where, noticeably, both phases have the same composition as the overall alloy [3].

Large magneto-volume effects (with anti-invar characteristics) were shown to be associated to the ferromagnetism of fcc-FeCu metastable alloys: while pure fcc-Fe (γ-Fe phase) is antiferromagnetic, it becomes ferromagnetic when its lattice is expanded as it is in some alloys [34, 35]. This behavior of

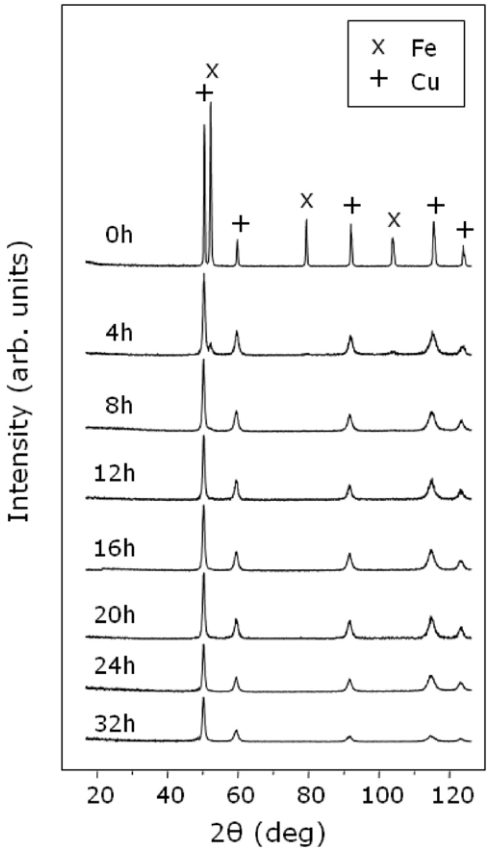

Figure 1. XRD patterns as a function of milling time.

Fe-rich nanosized precipitates could be understood in terms of recent *ab initio* calculations [37–39] that justify and generalize the Weiss two-state model for γ-Fe [43], where the high spin state magnetic moment of Fe can reach values over 2.5 μ_B. The coexistence of the two spin states was recently confirmed by x-ray magnetic circular dichroism studies of fcc-FeCu alloys [40]. The Curie temperature of fcc-FeCu alloys is found to change considerably with the Fe concentration, with characteristics of percolation behavior above ∼18 at.% Fe [9, 8, 29]. It increases up to ∼500 K for 60 at.% Fe.

The magnetic behavior of the Fe–Cu alloys near the Curie temperature and the anomalies accompanying the magneto-volume transformations are not yet completely understood. Moreover, an analysis of the ferromagnetic ordering of the paramagnetic state and the relation(s) with the nanoscale segregation in fcc-FeCu alloys is still lacking, mainly because atomic-level mixing and the possible development of short to medium range clustering in alloys made of elements which show little or no mutual solubility are often difficult to characterize experimentally [1]. In the following, we describe the characterization by x-ray diffraction, Mössbauer spectroscopy and magnetization measurements of a nanostructured fcc Cu-rich Fe–Cu alloy prepared by milling an elemental powder mixture of $Fe_{23}Cu_{77}$. Structural characteristics of the investigated alloy at the nanoscale are inferred from its magnetic properties. The emphasis is on the effect of clustering on the nature of the interacting magnetic entities.

2. Experimental details

Following the preparation method of $Fe_{50}Cu_{50}$ alloys we used in a previous work [33], $Fe_{23}Cu_{77}$ alloys were synthesized by mechanical alloying of Fe and Cu powders with nominal purity of 99% and average particle size of 60 μm and 150 μm, respectively. Milling was performed in a planetary ball-mill (Fritsch Pulverisette P6) in argon using hardened steel vial (250 ml) and balls (15 balls with 20 mm diameter each). A ball-to-powder weight ratio of 20:1 was used. The disk rotation speed was 200 rpm.

The evolution of the alloying process with milling time was followed by means of electron probe microanalysis (EPMA), x-ray diffraction (XRD), and ^{57}Fe Mössbauer spectroscopy. The x-ray diffraction patterns were obtained using Co Kα radiation ($\lambda = 0.178\,89$ nm). The mean crystallite sizes and microstrains were obtained from the widths of XRD peaks using the Williamson–Hall method [44].

Mössbauer spectra were recorded at room temperature (RT) in transmission geometry with a spectrometer operating in conventional constant acceleration mode. A Mössbauer spectrum was recorded at 82 K for the sample ground for 20 h. A ^{57}Co source in an Rh matrix with strength of ≃10 mCi was used. The spectra were analyzed by a constrained Hesse–Rübartsch method [45], which extracts a hyperfine magnetic field distribution, $P(B_{hf})$, from an experimental spectrum. Lorentzian line-shapes were employed in this procedure. The ^{57}Fe isomer shifts are given with respect to bcc α-Fe at RT.

Magnetization measurements were performed between 4.2 and 350 K, using a superconducting interference device (SQUID) magnetometer, for samples ground for 16 and 20 h.

3. X-ray diffraction and Mössbauer studies

Several samples were obtained for different milling times. Microprobe analysis shows that they are homogeneous at a micrometer scale. At 32 h of milling the measured composition is 24.2 ± 0.5 at.% Fe.

The x-ray diffraction patterns of the mechanically alloyed (MA) samples are shown in figure 1 as a function of milling time. A broadening of the diffraction peaks of both Fe and Cu occurs gradually with increasing milling time, as shown in figure 2. The intensities of the diffraction peaks of Fe decrease more rapidly than those of Cu do. The peaks of Fe are no longer observed after 12 h of milling. Fe is incorporated in the fcc-Cu structure, giving rise to a fcc-Cu(Fe) solid solution in accordance with the literature results. The lattice parameter of the obtained fcc-Cu(Fe) solid solution is equal to 0.3630 nm, which agrees with $a = 0.363$ nm measured by Ma *et al* [18] in a related MA alloy and by Sumiyama *et al* [8] in a sputtered film. The lattice is expanded with respect to Cu for which $a = 0.3615$ nm. The incorporation of iron in the fcc lattice of copper occurs in the first hours of milling, as shown in figure 2 by the decrease of the angle of the Cu(111) diffraction peak as a function of time with a concomitant peak broadening. The crystallite size and microstrain in the stationary state of the milled powders, determined by x-ray analysis, are 16 nm and 0.9%, respectively.

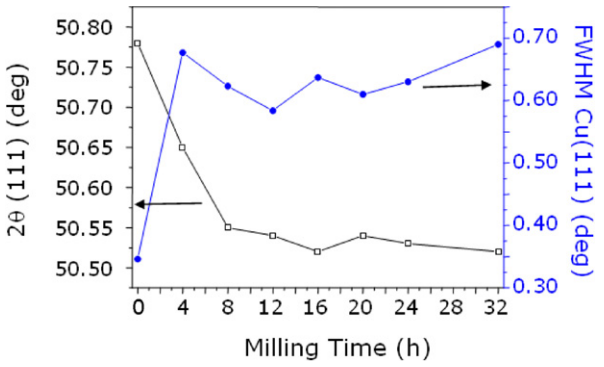

Figure 2. Angular position (2θ) of the (111) peak of the fcc Cu phase and corresponding FWHM (deg) as a function of milling time.

Figure 3 shows transmission RT Mössbauer spectra of the milled samples. Two different main components can be observed: a doublet attributed to a Cu-rich fcc-Cu(Fe) phase which is paramagnetic-like at RT and a sextuplet attributed to bcc α-Fe which is progressively incorporated into the fcc-Cu(Fe) phase. The RT hyperfine parameters of the doublet due to fcc $Fe_{23}Cu_{77}$ are IS $=$ 0.145 mm s^{-1} and QS $=$ 0.46 mm s^{-1}. The quadrupole splitting agrees with literature results as QS $=$ 0.49 mm s^{-1} [19] and QS $=$ 0.45 mm s^{-1} for mechanically alloyed fcc $Fe_{25}Cu_{75}$ and fcc $Fe_{30}Cu_{70}$ [30] respectively. Further, a QS of 0.38 mm s^{-1} was measured at RT from a slightly asymmetric doublet for a sputtered film of fcc $Fe_{26}Cu_{74}$ [10].

Assuming that the Mössbauer f-factor is the same for both components, the following magnetic fractions were obtained: 63%, 16.6%, 5%, 5%, 6.4%, and 11% for 4 h, 8 h, 16 h, 20 h, 24 h, and 32 h of milling, respectively. These results suggest that a steady state is really obtained after ∼16 h of milling and that the increase of the α-Fe fraction for milling times longer than ∼24 h is due to contamination by steel of milling tools. Indeed, the contamination rate may change with milling time as the mechanical properties of ground powders evolve with it because of alloying and because of the effect of the grain size decrease (Hall–Petch relation). The samples were found to be homogeneous from the point of view of x-ray diffraction for powders milled for times ranging from 16 to 24 h. A Mössbauer spectrum recorded at 82 K (figure 4) shows that the sample milled for 20 h is magnetic, as expected with a small additional contribution from α-Fe (∼4%, $H = 33.8$ T).

The mean isomer shift is $\langle \mathrm{IS} \rangle = 0.24$ mm s^{-1}. The main broad part of the hyperfine field distribution has an overall Gaussian aspect whose maximum is at $\langle H \rangle_{\mathrm{peak}} = 17.4$ T while the mean hyperfine field is $\langle H \rangle = 14$ T. It is the intense central part, with fields below 3 T (figure 4), which explains the significant difference between these two fields. The 4.2 K spectra published in the literature for compositions close to the one investigated here prove that the observed low temperature broadening is heterogeneous and is due to a static distribution of magnetic hyperfine fields. However, the existence of the relatively intense central 'doublet' observed here at 82 K very likely originates from relaxation phenomena yielding spectral shapes similar, for instance, to those calculated for an Au(Fe)

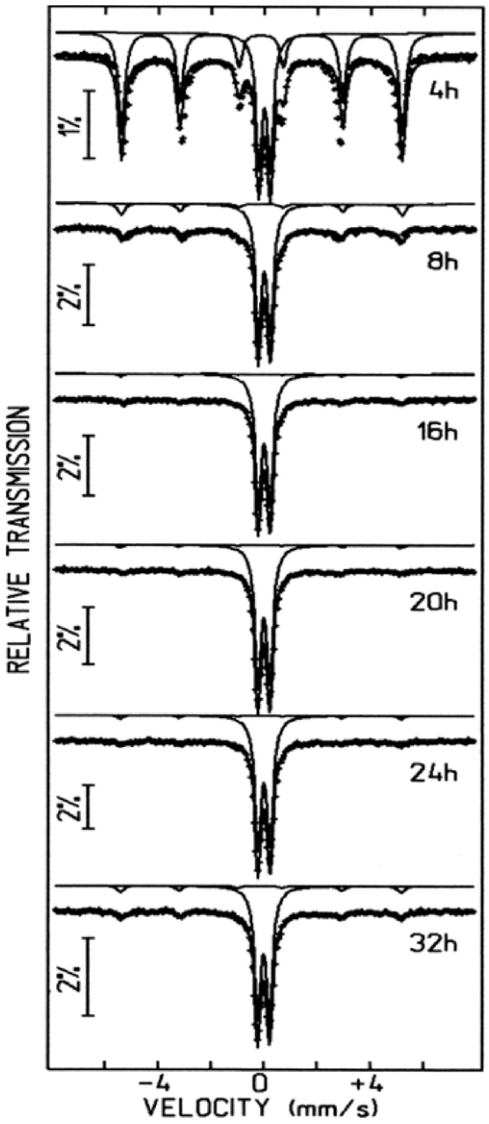

Figure 3. Mössbauer spectra at room temperature as a function of cumulative milling time.

spin glass [46]. A rather similar spectrum, but with a less intense central part, is seen for sputtered $Fe_{26}Cu_{74}$ (T_C ∼ 240 K) at 160 K, in a temperature range where the field varies strongly with T [10]. Rather similar fields, although somewhat larger, with values of 22 T, 20 T, 21.6 T, and 22 T are reported at 77 K for MA $Fe_{20}Cu_{80}$ [36], $Fe_{25}Cu_{75}$ [19], and $Fe_{30}Cu_{70}$ (T_C ∼ 380 K [30]) samples and at 83 K for MA $Fe_{30}Cu_{70}$ (T_C ∼ 300 K [31]), respectively. By contrast, much smaller mean fields of ∼7 T and ∼8 T at 4.2 K are obtained from figure 4 of [9] for sputtered $Fe_{20}Cu_{80}$ at.% and $Fe_{30}Cu_{70}$ at.% respectively. Finally, $\langle H \rangle_{\mathrm{peak}} = 23.8$ T and $\langle H \rangle = 20.6$ T are measured at 82 K for sputtered $Fe_{26}Cu_{74}$ from figure 3 of [10]. The fields $\langle H \rangle_{\mathrm{peak}}(T)$ and $\langle H \rangle(T)$ of the latter alloy vary anomalously when T decreases below T_f ∼ 380 K as they increase much more than expected from an extrapolation of their behaviors between T_f and T_C. These increases are ascribed to a freezing of transverse Fe-spin components below a spin-canting transition at T_f [10]. The field differences reflect the strong sensitivity of $\langle H \rangle(T)$ and of the magnetic properties

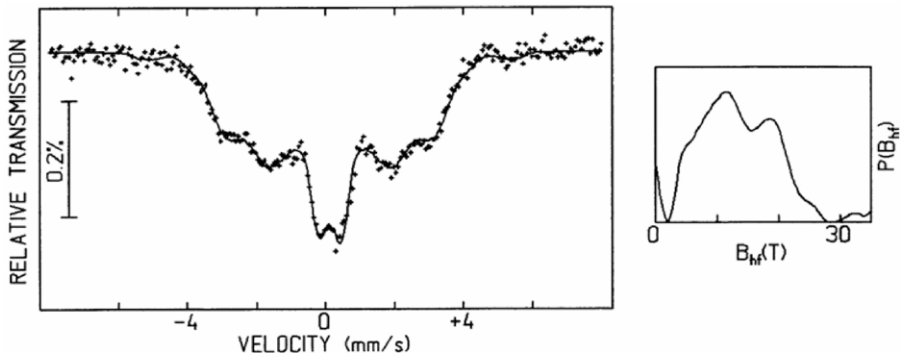

Figure 4. Mössbauer spectrum at 82 K and the corresponding hyperfine field distribution of the sample milled for 20 h.

of such metastable alloys both on preparation methods and on the Cu content.

4. Magnetization studies

Figure 5 shows the temperature dependence of the low field magnetization M for samples milled for 16 and 20 h. The measurements were performed in increasing temperatures, after cooling under zero magnetic field and applying the measurement field ($H = 50$ Oe) at the lowest temperature (10 K) (ZFC procedure). The field cooled procedure (FC) corresponds to measurements taken after cooling the sample from 300 to 10 K with the measurement field applied. The temperature dependence of M reveals the ferromagnetism of the two as-milled Fe–Cu alloys, which both order at similar temperatures: $T_C \sim 220$ K. This Curie temperature agrees well with that found for $x = 23$, from the composition dependence of T_C of MA Fe_xCu_{100-x} measured by Socolovsky *et al* [29], and with that reported by Martínez-Blanco *et al* [42] for $x = 25$. For sputtered alloys [8, 9], the Curie temperature is systematically lower than that measured for the MA alloy of the same composition. It is, for instance, ∼120 K for $x = 25$ [9] and ∼185 K for $x = 23$ [8]. Moreover, the behavior at the highest temperatures of measurements of the present work indicates the presence of a limiting residual magnetization, associated with the presence of bcc α-Fe. The thermal irreversibility observed in both samples reveals the existence of interactions among the Fe atoms that are not in the form of α-Fe. As will become evident in the following discussion, this irreversibility is associated with ferromagnetic interactions between Fe-rich clusters.

To analyze the nature of the magnetic state, the field dependence of the magnetization of the 20 h sample, was also studied in the temperature range without irreversibility, from 230 to 350 K. Besides the Fe–Cu contribution, one finds a temperature independent remnant magnetization, $M_r = 0.28$ emu g^{-1} for $H = 50$ Oe. To confirm that it is associated with a residual bcc α-Fe content in the sample, we performed an additional $M(T)$ measurement, at an applied field $H = 1000$ Oe, large enough to saturate α-Fe. We find that at high temperatures this $M(T)$ curve can be modeled by a Curie–Weiss term (associated with the Fe–Cu alloy) plus a constant $M_{sat} = 0.55 \pm 0.03$ emu g^{-1} that corresponds to ∼0.03 μ_B/Fe

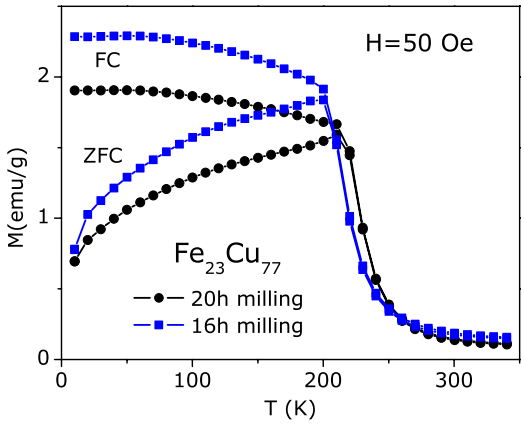

Figure 5. Temperature dependence of low-field (50 Oe) magnetization M, of the samples milled for 16 h and for 20 h.

i.e. ∼1.3% of α-Fe. This value is apparently lower than that obtained by Mössbauer spectroscopy but the latter technique is selective and measures the fraction of the total Fe amount in the α-Fe phase, namely 5% with the assumption that the f-factors at RT are the same for the fcc and the bcc phases. Then the bcc phase includes ∼1.2% of all atoms. This α-Fe contribution can be subtracted as a constant contribution for $H \gtrsim 500$ Oe (after α-Fe saturation) and the Fe–Cu part can be further studied. In the following we will present the analysis of the Fe–Cu magnetization $M = M_{raw} - M_{sat}$, valid for magnetic fields larger than ∼500 Oe (figure 6).

In a previous work, the magnetic properties of Fe–Cu alloys were analyzed with an oversimplified superparamagnetic model that considers the contribution of non-interacting magnetic clusters, following the Langevin function, whose moment was temperature dependent [47]. Deviations of the magnetization curves of as-milled $Fe_{25}Cu_{75}$ from a single Langevin function below 300 K, with differences increasing with decreasing measuring temperature are reported too by Eilon *et al* [19]. Indeed, such simple analyses are not compatible with the existence of a critical Curie temperature, T_C, and one should not ignore the associated magnetic interactions. This implies the use of the concept of superferromagnetism, introduced in several contexts (oxide or metal dispersed particles) to generalize the superparamagnetic description to include a molecular field [48–51]. For that purpose, we described the

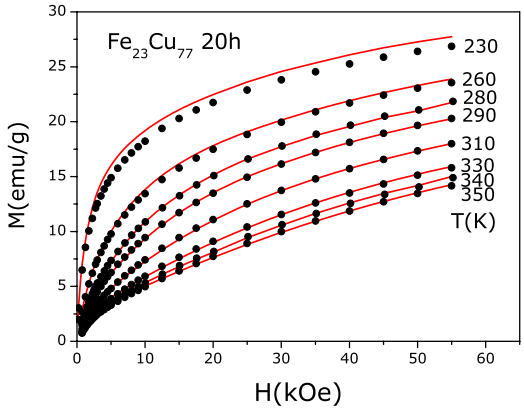

Figure 6. Field dependence of the Fe–Cu magnetization of the sample milled for 20 h in the range $H > 500$ Oe, after removing the contribution $M_{sat} = 0.55 \pm 0.03$ emu g^{-1}, due to the α-Fe phase. Solid lines are calculated using the molecular field model, as discussed further in the text. Calculations for $T = 230$ K are also included, although data lie outside the scaling range.

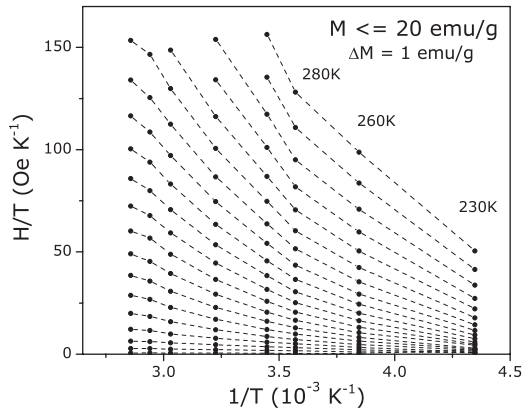

Figure 7. H/T versus $1/T$ representation of interpolated M versus H data at constant magnetization values (lines join data at 1 emu g^{-1} step), used to determine the molecular exchange field. The data at $T = 230$ K are clearly out of the region where the mean field approach can be used.

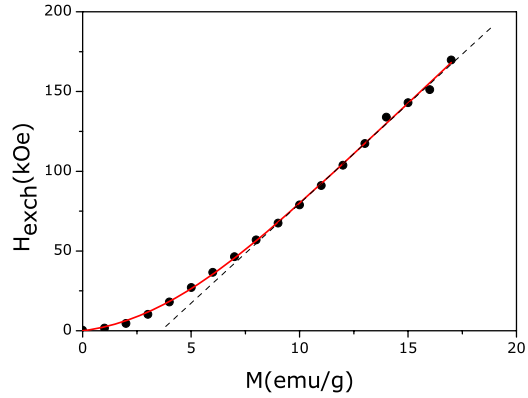

Figure 8. Molecular exchange field H_{exch} as a function of the magnetization M. The full curve is an interpolating fifth degree polynomial. The dashed line points to a limiting linear regime at higher magnetizations.

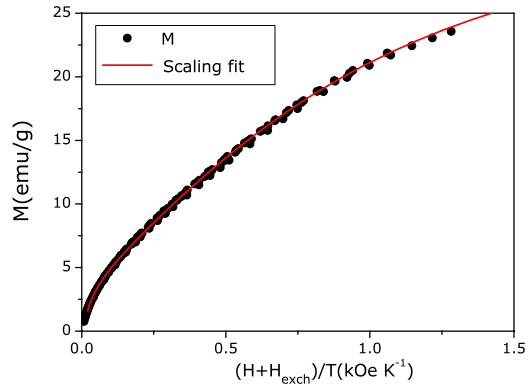

Figure 9. Scaling plot of the magnetization data for $T \geqslant 260$ K, as a function of the scaling variable, using the interpolated H_{exch}.

data using a recently developed method based on a ferromagnetic mean field model [52]. To analyze the data, we assume that the interactions can be approximated by a molecular exchange field, H_{exch} and that the magnetization can be scaled by $M = f((H + H_{exch})/T)$, where f is an *a priori* indeterminate scaling function (for instance, a Brillouin function in a single ion approach). H_{exch} is also an *a priori* unknown function of the magnetization M (linear, in the simple molecular field picture) determined so as to ensure the scaling of the data. After this scaling is obtained, both the f function and H_{exch} can be further considered to get their physical meaning.

Following the scaling method, one starts by analyzing interpolated M versus H data for constant magnetization values by plotting H/T versus $1/T$. This is done in figure 7 at 1 emu g^{-1} steps. The slope of the linear portion of each isomagnetic curve (from highest temperatures to a lower limit, ~280 K) is used to determine the molecular exchange field H_{exch} as a function of M. One notices that the data at $T =$ 230 K, close to the Curie temperature, are clearly out of the temperature region where the mean field approximation can be strictly used, within statistical fluctuations of the data. For higher magnetizations, above 18 emu g^{-1}, the linear relations are not reliable, as there are not enough points. This limits our analysis to the range shown in figure 8. A striking outcome of the analysis is that instead of the more common linear dependence of H_{exch} as a function of the magnetization M, one finds a much steeper dependence, which cannot be simply described even by a third order polynomial [52]. At higher magnetizations, one finds a limiting linear regime (dashed line) but that does not go through the origin. To continue to apply and check the validity of the mean field model, one has to be able to describe the function $H_{exch}(M)$. The full curve in figure 8 corresponds to a fifth degree polynomial interpolation, which is taken as a convenient intermediate fitting function. The plot of the magnetization data for $T \geqslant 260$ K as a function of the scaling variable $(H + H_{exch})/T$ is presented in figure 9. The scaling is observed to be very efficient from $T = 350$ K down to 260 K, the data deviate slightly only at higher magnetizations.

Although the scaling was expected to be reliable for magnetizations below about 17 emu g^{-1}, the collapse of the

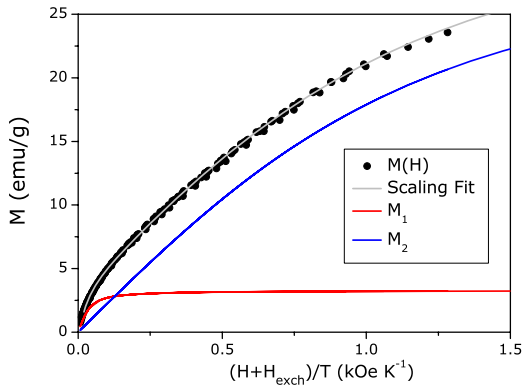

Figure 10. Scaling plot of the magnetization data for $T \geqslant 260$ K, including the fitted f function which is a sum of two Langevin contributions (shown separately) as a function of the scaling variable.

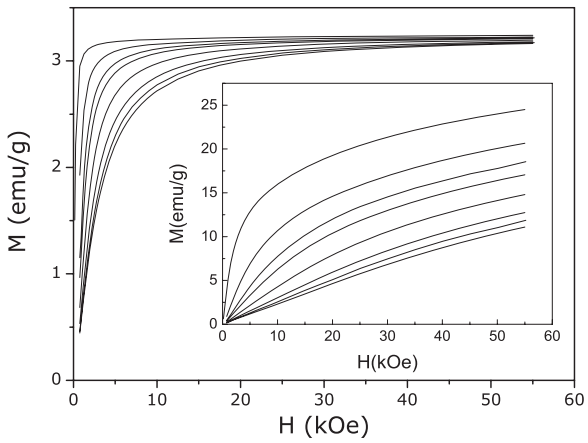

Figure 11. Calculated magnetization curves of the two Langevin contributions M_1 and M_2 (inset) obtained using the molecular field model. Data for $T = 230$ K are also included although they lie outside the scaling range.

data to a single scaling line seems valid for values up to about 23 emu g^{-1}. This shows that the molecular exchange field dependence was well described in all that range and even well extrapolated beyond the expected range of validity of the fitting function. The scaling function f, now determined as a function of its natural variable, can be examined consistently by fitting it to some particular model. The shape of $f(x)$ suggests immediately that it cannot be reasonably accounted for by a single Langevin function. However, $f(x)$ can be fitted by a simple model of a sum of two Langevin contributions:

$$M(H,T) = M_{S1} L_{\mu_1}\left[\frac{(H+H_{exch})}{T}\right] + M_{S2} L_{\mu_2}\left[\frac{(H+H_{exch})}{T}\right], \quad (1)$$

for two quite distinct populations of magnetic clusters with different sizes where M_{S1}, μ_1 and M_{S2}, μ_2 are the associated saturation magnetizations and magnetic moments. For each, the ratio M_{Si}/μ_i allows us to obtain the respective cluster density (number of clusters per unit mass). The Langevin function for each population:

$$L_\mu(x) = \coth\left(\frac{\mu x}{k_B}\right) - \frac{k_B}{\mu x}. \quad (2)$$

The fitted scaling function is presented in figure 10 for $T \geqslant 260$ K, along with the contributions of the two populations of clusters. The fitting parameters are presented in table 1 (including in the error the difference from fits with and without the $T = 260$ K data) along with the average volume density and estimated distance between clusters belonging to the same family. The larger clusters exhibit a very rapid increase of the magnetization, saturating at values of the order of 10% of the total magnetization. By contrast, the smaller clusters account for 90% of the magnetization and for the slow increase of the magnetization observed in fields up to several kOe.

Moreover, the total saturation magnetization obtained from the fit performed in the paramagnetic phase ($M_{S1} + M_{S2} = 35.9$ emu g^{-1}), using experimental data values below 25 emu g^{-1}, compares well with the saturation magnetization

Table 1. Saturation magnetization, magnetic moment, average volume density, and inter-cluster distance for the two cluster populations.

	M_S (emu g^{-1})	μ (μ_B)	N (cm^{-3})	D (nm)
M_1 (large cluster)	3.25 ± 0.05	860 ± 20	3.5×10^{18}	6.6
M_2 (small cluster)	32.6 ± 0.03	30.5 ± 0.5	9.9×10^{20}	1.0

of the $Fe_{23}Cu_{77}$ sample milled for 20 h, 39.8 emu g^{-1}, measured at $T = 4.2$ K, subtracting M_{sat} from α-Fe (results not shown). The magnetization curves can be reconstructed from the fit and are shown in figure 6, where the solid lines are calculated using the molecular field model for each temperature. Values for $T = 230$ K, which are situated outside the scaling range, are also included. Figure 11 shows the calculated magnetization curves of each of the two Langevin contributions.

5. Discussion and conclusion

5.1. Structure of concentrated Fe–Cu alloys

As emphasized by Ma [1], the non-equilibrium alloys created in systems with positive enthalpies of mixing have to survive a thermodynamic driving force for phase decomposition. Therefore, true atomic-level alloying and the chemical homogeneity of the two constituents cannot be taken for granted but they are most often difficult to prove [1]. The difficulty in ascertaining whether a single-phase homogeneous alloy is formed or not from XRD patterns is further discussed by Ma [1] (see too [53]). A telling example of the difficulty to characterize the very 'microstructure' is that of concentrated bcc $Fe_{1-x}Cr_x$ alloys, with typical Cr contents ranging between ~0.3 and ~0.7, mechanically alloyed in a planetary ball-mill, which were repeatedly reported to be homogeneous from x-ray diffraction and Mössbauer spectroscopy studies. Thanks to magnetic measurements, an as-milled bcc $Fe_{0.30}Cr_{0.70}$ alloy was shown to exhibit intragranular composition fluctuations, with an amplitude of about 0.10 at a scale of ~2 nm, in

its stationary state. Indeed, these nanoscale fluctuations, which escape detection by XRD and Mössbauer spectroscopy, are evidenced without ambiguity through their effect on magnetization and ac magnetic susceptibility (see figure 2 of [54]). They differ from those found for a macroscopic phase separation. Ac susceptibility measurements demonstrate further that, for the milling conditions at work in [54, 55], a ball-milled elemental powder mixture of Fe and Cr and a ground as-cast alloy, both with the $Fe_{0.30}Cr_{0.70}$ composition, reach the same stationary state with nanoscale decomposition features [55].

Stationary states reached in such off-equilibrium conditions are expected to depend on the precise dynamical conditions as concluded for instance from the theory of driven alloys [2]. Different ball-mills with different milling conditions (temperature, injected power, shock versus friction) may thus lead to different stationary states with different atomic distributions at the nanoscale. Atoms in ball-milled alloys, like the Fe–Cu alloys investigated here, change their environment both as a result of the motion of dislocations, either perfect or partial according to the grain size, and of mechanical twinning [2]. Twinning is a common deformation mechanism of nanocrystalline fcc alloys during ball-milling, even when their stacking fault energy is high [56].

An inverse grain size effect on twinning has been recently reported to occur for nanocrystalline fcc Ni [57]. Decreasing the grain size first promotes twinning and then hinders it for grain sizes below 20–30 nm. By contrast, such an effect does not exist for the slips of partial dislocations which produce stacking faults [57].

Multiple twinning is also frequent in those nanocrystalline metals which show a strongly enhanced twinning propensity. Fivefold twins are, for instance, observed to form in small grains and are explained by a sequential twinning mechanism resulting from the emission of a series of partial dislocations by grain boundaries [58, 59]. high-resolution transmission electron microscopy (HRTEM) evidences a number of deformation twins in MA $Fe_{16}Cu_{84}$ [60]. Wu *et al* [61] discovered recently that the vast majority of deformation twins in nanocrystalline fcc metals (Al, Ni, Cu) yield zero macroscopic strain and contribute to the bulk deformation by favorably reorienting the grains. They proposed a new twinning mechanism which requires lower activation stresses than those needed for twins contributing to the macroscopic strain.

The contribution of dislocation motion and of twinning may depend on the nature of shocks (tangential or normal shocks) which depends in turn on the type of mill. The fact that different structural characteristics of as-milled alloys are reported for the same alloy composition is therefore not surprising for systems whose strong trend is to phase separate. The way the issue is forced [1] by employing highly non-equilibrium processing to overcome the effects of the positive enthalpy of mixing is reflected for instance in the significant differences mentioned at the end of section 3 between the hyperfine magnetic properties of Fe–Cu alloys prepared either by ball-milling or by sputtering.

That true alloying occurs at the atomic scale in fcc Cu–Fe is a well-established fact. Our x-ray and Mössbauer results agree with that fact. Harris *et al* [21] characterized concentrated Fe–Cu alloys, mechanically alloyed either in a Spex mill or in a vibratory mill, by EXAFS experiments at the Fe and Cu K absorption edges. They concluded that both Fe and Cu atoms reside in a fcc phase where the first coordination sphere consists of a mixture of Fe and Cu atoms in a ratio which reflects the alloy composition. Heterogeneities were reported to exist from an HRTEM study [60] and from a three-dimensional atom probe investigation [28] of mechanically alloyed $Fe_{16}Cu_{84}$ and $Fe_{20}Cu_{80}$ respectively, both prepared in planetary ball-mills as done here. Nanoscale analysis of an MA $Fe_{16}Cu_{84}$ yielded the expected average composition but different Fe contents were found according to grain size, the smaller the grain size, the higher the Fe content [60]. Even after apparent complete alloying, very small bcc domains with size near 1 nm were observed in the latter alloy. Similar conclusions were obtained with a three-dimensional (3D) atom probe for mechanically alloyed and compacted $Fe_{20}Cu_{80}$ [28]. Small-angle x-ray scattering experiments in MA Fe_xCu_{100-x} ($14.1 \leqslant x \leqslant 45$) were interpreted in terms of scattering by 'objects' dispersed in a nearly pure Cu matrix. Their main size is 2 nm and their composition is $Fe_{35}Cu_{65}$ whatever x. We notice finally that Hernando *et al* [14] and Crespo *et al* [15] concluded from magnetization and Mössbauer measurements that part of the Fe obtained by heating a $Fe_{51}Cu_{49}$ alloy is neither in the bcc form nor in the original fcc solid solution with Cu. Such heated alloys exhibit a variety of magnetic behaviors related to composition fluctuations produced by spinodal decomposition. The fact that heterogeneities, nanoscale composition fluctuations among others, occur in ball-milled samples according to the injected power, as seen for Fe–Cr alloys too [54, 55], may thus be considered.

5.2. Interpretation of magnetic measurements and structural consequences

Although the scaling analysis seems to yield an overall consistent description of the data, it is essential to understand the very unusual magnetization dependence of the exchange field. The presence of a bimodal distribution of magnetic nanoclusters with quite distinct densities and saturation values gives a clue to the physical meaning. In fact, for a total magnetization higher than $\sim$7 emu g^{-1}, the contribution from M_1 is saturated (constant). This is the region above which $H_{\rm exch}(M)$ becomes linear (figure 8). Figure 12 shows the molecular exchange field $H_{\rm exch}$ plotted as a function of M_2, the low moment Langevin component of the magnetization (smaller clusters), obtained from the fitting.

A linear relation is indeed found, except for a very small curvature for the highest values, so that one can confidently define a molecular field parameter λ_2 such that $H_{\rm exch} = \lambda_2 M_2$. The slope of the line is the same as the one obtained at higher magnetizations in figure 8: $\lambda_2 \sim 1.2 \times 10^4$ Oe g emu^{-1}. One may infer from this result that only M_2 contributes significantly to the magnetic interactions in the investigated fcc FeCu alloy (for both the M_1 and M_2 components), probably because of the much lower density of the large clusters. The mechanism supporting the superferromagnetic state in which there is

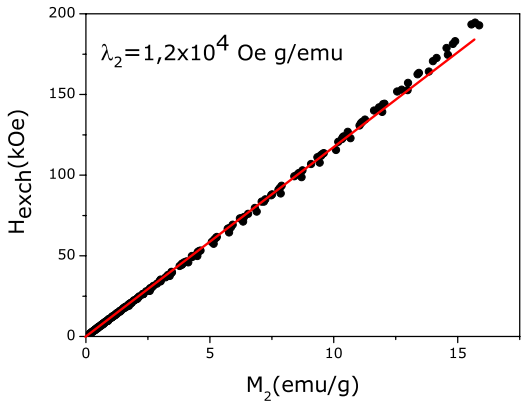

Figure 12. Molecular exchange field H_{exch} as a function of M_2, the low moment Langevin component of the magnetization obtained from the fitting. The line has the same slope as the one observed at higher magnetizations in figure 8.

magnetic percolation of the smallest clusters without physical percolation (as the average inter-cluster distance is estimated to be ∼1 nm) is most probably the mediation by the conduction electrons of the matrix. These two cluster populations point to a heterogeneous alloy 'microstructure'. We notice indeed that a perfectly mixed and disordered fcc $Fe_{23}Cu_{77}$ would be a classical transition metal ferromagnet. Further, techniques of structural characterization like HRTEM [60] or 3D atom probing [28], applied to ball-milled fcc Fe–Cu alloys, led us to conclude that such alloys are heterogeneous.

Multiple twinning, discussed in section 5.1, also plays an important role in isolated nanoparticles. Indeed, bulk fcc transition metals are known to form multiply twinned particles such as icosahedra or decahedra when they become nanosized ([62] and references therein). In a recent study, Rollmann *et al* [63] showed by *ab initio* calculations that isolated Fe nanoclusters are more stable in fcc-like structures (icosahedral/cuboctahedral) below about 100 atoms, while bcc-like structures are favored for larger clusters while their cores retain, however, the small cluster structure. They present a ferromagnetic or a ferrimagnetic spin ordering, related to the high and low spin states.

The bimodal cluster size distribution evidenced by our magnetic measurements is estimated to consist of small clusters with a radius of ∼0.5 nm (∼11–16 Fe atoms), and of larger clusters with a radius of ∼1.5 nm (∼400–450 Fe atoms). This value is obtained from the magnetic moment per Fe atom and the sample density (8.6 g cm^{-3}). The uncertainty mainly results from the assumed value of the atomic magnetic moments for each cluster type, which are taken to be in the range 1.94–2.9 μ_B/Fe atom for the smaller clusters and 1.94–2.2 μ_B/Fe atom for the larger clusters. The lower value is obtained from the total saturation magnetization measured at 4.2 K (40.4 emu g^{-1}, including the α-Fe phase contribution), giving an average moment of 1.94 μ_B/Fe atom for the whole sample. The higher limits are estimated as follows: studies of Fe clusters present a decrease of atomic magnetic moment with cluster size, with values reaching 2.9 μ_B/Fe atom in the case of clusters below about 25 atoms [63]. On the other hand, our larger clusters should approach the average value, but clusters with a few hundred Fe atoms are reported [63] to still have higher than bulk magnetic moment (2.2 μ_B/Fe atom). Values in this range are reported in analogous studies of MA Fe–Cu alloys: a moment of 2.3–2.4 μ_B/Fe atom is reported by Eilon *et al* [19] for $Fe_{25}Cu_{75}$. Mashimo *et al* [34] give 2.07 μ_B for MA and shock consolidated $Fe_{30}Cu_{70}$, Mazzone *et al* [20] give 2.26 μ_B for as-milled $Fe_{30}Cu_{70}$, Yousif *et al* [36] give an experimental value of 3.05 μ_B and a theoretical value of 2.65 μ_B for $Fe_{20}Cu_{80}$. A value of 2.23 μ_B/Fe atom is obtained for Fe_xCu_{100-x} from $\mu = 2.85(x-5)/x$ μ_B/Fe atom by Bove *et al* [64].

To appear and to interact magnetically as distinct and separated objects, the clusters must be Fe-rich with an Fe-depleted matrix surrounding them. This condition should be verified more promptly in the case of the smaller clusters, which are expected to have higher than average Fe content. Therefore, although the magnetic clusters we consider are embodied in a bulk matrix, the small clusters might be similar to the icosahedral or fcc cuboctahedra cluster (13 atoms), which are particularly stable [63] while the large ones may correspond to Cu-stabilized fcc clusters. The existence of very small grains (1 nm) cannot, however, be excluded from the HRTEM and 3D atom probe observations reported in the literature [28, 60]. In FeCu alloys, the presence of Cu atoms in the fcc-Fe clusters should help stabilizing the fcc nanophase beyond these sizes, at least at temperatures below the magneto-volume transformations, which occur much above room temperature, at $T \sim 500$ K [37–39]. The inhomogeneous structure of the clusters, with a progressive deformation (probably relaxed with respect to the matrix), by the incorporation of Cu atoms, is probably fundamental to the high magnetic moment and magneto-volume effects in these alloys.

In conclusion, our study reveals that the $Fe_{23}Cu_{77}$ alloy has a mean grain size of ∼16 nm and that it is heterogeneous. From our magnetic measurements, we conclude that grains contain magnetic Fe-rich nanoclusters with a bimodal size distribution. The smaller clusters comprise about 14 atoms, close to a 13 atom icosahedral/cuboctahedral arrangement which is found in multiply twinned and isolated nanoparticles of fcc transition metals and of bcc Fe. The inter-cluster ferromagnetic interactions that lead to a Curie temperature $T_C \sim 220$ K can be described by a mean field determined by the smaller clusters only, which account for 90% of the magnetization.

Acknowledgments

N J O Silva and J S Amaral acknowledge scholarships by FCT (SFRH/BD/10383/2002 and SFRH/BD/17961/2004 respectively). This work is partially supported by project POCTI/CTM/61284/2004 from FCT and FEDER. The possibility of performing the SQUID magnetic measurements in the Materials Institute of the University of Porto (IFIMUP) is gratefully acknowledged. B F O Costa and G Le Caër gratefully acknowledge the financial support of the French–Portuguese bilateral program PESSOA (grant no. 14617RE).

References

[1] Ma E 2005 *Prog. Mater. Sci.* **50** 413–509
[2] Martin G and Bellon P 1997 *Solid State Phys.* **50** 189–331
[3] Schilling P J, Palshin V, Tittsworth R C, He J H and Ma E 2003 *Phys. Rev.* B **68** 224204
[4] Odunuga S, Li Y, Krasnochtchekov P, Bellon P and Averback R S 2005 *Phys. Rev. Lett.* **95** 045901
[5] Chien C L, Xiao J Q and Jiang J S 1993 *J. Appl. Phys.* **73** 5309–14
[6] Xiao J Q, Jiang J S and Chien C L 1992 *Phys. Rev. Lett.* **68** 3749–52
[7] Perez M, Perrard F, Massardier V, Kleber X, Deschamps A, de Monestrol H, Pareige P and Covarel G 2005 *Phil. Mag.* **85** 2197–210
[8] Sumiyama K, Yoshitake T and Nakamura Y 1984 *J. Phys. Soc. Japan* **53** 3160–5
[9] Chien C L, Liou S H, Kofalt D, Yu W, Egami T and Mcguire T R 1986 *Phys. Rev.* B **33** 3247–50
[10] Sumiyama K, Nishi K, Nakamura Y, Manns V, Scholz B, Privik M, Keune W, Stamm W, Dumpich G and Wassermann E F 1991 *J. Magn. Magn. Mater.* **96** 329–34
[11] Konno T J, Li D, Otomo T, Sumiyama K and Suzuki K 1998 *J. Phys. Soc. Japan* **67** 1498–9
[12] Uenishi K, Kobayashi K F, Nasu S, Hatano H, Ishihara K N and Shingu P H 1992 *Z. Metallk.* **83** 132–5
[13] Yavari A R, Desre P J and Benameur T 1992 *Phys. Rev. Lett.* **68** 2235–8
[14] Hernando A, Crespo P, Escorial A G and Barandiaran J M 1993 *Phys. Rev. Lett.* **70** 3521
[15] Crespo P, Hernando A, Yavari R, Drbohlav O, Escorial A G, Barandiaran J M and Orue I 1993 *Phys. Rev.* B **48** 7134–9
[16] Eckert J, Holzer J C and Johnson W L 1993 *J. Appl. Phys.* **73** 131–41
[17] Eckert J, Holzer J C, Krill C E and Johnson W L 1993 *J. Appl. Phys.* **73** 2794–802
[18] Ma E, Atzmon M and Pinkerton F E 1993 *J. Appl. Phys.* **74** 955–62
[19] Eilon M, Ding J and Street R 1995 *J. Phys.: Condens. Matter* **7** 4921–8
[20] Mazzone G and Antisari M V 1996 *Phys. Rev.* B **54** 441–6
[21] Harris V G, Kemner K M, Das B N, Koon N C, Ehrlich A E, Kirkland J P, Woicik J C, Crespo P, Hernando A and Escorial A G 1996 *Phys. Rev.* B **54** 6929–40
[22] Kaloshkin S D, Tomilin I A, Andrianov G A, Baldokhin U V and Shelekhov E V 1997 *Mater. Sci. Forum* **235** 565–70
[23] Jiang J Z, Gente C and Bormann R 1998 *Mater. Sci. Eng.* A **242** 268–77
[24] Hong L B and Fultz B 1998 *Acta Mater.* **46** 2937–46
[25] Xu J, Collins G S, Peng L S J and Atzmon M 1999 *Acta Mater.* **47** 1241–53
[26] Schilling P J, He J H, Tittsworth R C and Ma E 1999 *Acta Mater.* **47** 2525–37
[27] Crespo P and Hernando A 1999 *Recent Res. Dev. Nanostruct.* **1** 63
[28] Wanderka N, Czubayko U, Naundorf V, Ivchenko V A, Yermakov A Y, Uimin M A and Wollenberger H 2001 *Ultramicroscopy* **89** 189–94
[29] Socolovsky L M, Sanchez F H and Shingu P H 2001 *Hyperfine Interact.* **133** 47–52
[30] Principi G, Spataru T, Gupta R, Enzo S, Kuncser V and Filoti G 2001 *J. Alloys Compounds* **326** 188–92
[31] Ino H, Hayashi K, Otsuka T, Isobe D, Tokumitsu K and Oda K 2001 *Mater. Sci. Eng.* A **304** 972–4
[32] Fernandéz van Raap M B, Socolovsky L M, Sanchez F H and Torriani I L 2002 *J. Phys.: Condens. Matter* **14** 857–64
[33] Lucas F M, Trindade B, Costa B F O and Le Caer G 2002 *Mater. Sci. Forum* **230–2** 631–4
[34] Mashimo T, Huang X S, Fan X, Koyama K and Motokawa M 2002 *Phys. Rev.* B **66** 132407
[35] Gorria P, Martinez-Blanco D, Blanco J A, Hernando A, Garitaonandia J S, Barquin L F, Campo J and Smith R I 2004 *Phys. Rev.* B **69** 214421
[36] Yousif A, Bouziane K, Elzain M E, Ren X, Berry F J, Widatallah H M, Al Rawas A, Gismelseed A and Al-Omari I A 2004 *Hyperfine Interact.* **156** 213–21
[37] Palacios S L, Iglesias R, Martinez-Blanco D, Gorria P, Perez M J, Blanco J A, Hernando A and Schwarz K 2005 *Phys. Rev.* B **72** 172401
[38] Gorria P, Martinez-Blanco D, Blanco J A, Perez M J, Hernando A, Barquin L F and Smith R I 2005 *Phys. Rev.* B **72** 014401
[39] Gorria P, Martinez-Blanco D, Blanco J A, Perez M J, Gonzalez M A and Campo J 2006 *Physica* B **384** 336–40
[40] Orecchini A, Sacchetti F, Petrillo C, Postorino P, Congeduti A, Giorgetti C, Baudelet F and Mazzone G 2006 *J. Alloys Compounds* **424** 27–32
[41] Iglesias R and Palacios S L 2007 *Acta Mater.* **55** 5123–7
[42] Martinez-Blanco D, Gorria P, Perez M J, Blanco J A and Gonzalez M A 2007 *J. Non-Cryst. Solids* **353** 859–61
[43] Weiss R J 1963 *Proc. Phys. Soc.* **82** 281
[44] Williamson G K and Hall W H 1953 *Acta Metall.* **1** 22–31
[45] Le Caër G and Dubois J M 1979 *J. Phys. E: Sci. Instrum.* **12** 1083–90
[46] Meyer C, Hartmann-Boutron F, Gros Y and Campbell I A 1985 *J. Magn. Magn. Mater.* **46** 254–66
[47] Costa B F O, Amaral V S, Silva N J O and Le Caer G 2004 *Proc. 7th Int. Conf. on Nanostructured Materials* p 73
[48] Kündig W, Ando K J, Lindquist R H and Constabaris G 1967 *Czech. J. Phys.* **17** 467
[49] Bostanjoglo O and Rohkel K 1971 *Phys. Status Solidi* a **7** 387
[50] Kokorin V V, Osipenko I A, Polotnyuk V V, Zolkina S V and Shirina T V 1982 *Fiz. Met. Metalloved.* **54** 48–53
[51] Mørup S, Madsen M B, Franck J, Villadsen J and Koch C J W 1983 *J. Magn. Magn. Mater.* **40** 163–74
[52] Amaral J S, Silva N J O and Amaral V S 2007 *Appl. Phys. Lett.* **91** 172503
[53] Michaelsen C 1995 *Phil. Mag.* A **72** 813–28
[54] Delcroix P, Ziller T, Bellouard C and Le Caer G 2001 *Mater. Sci. Forum* **360–3** 329–36
[55] Le Caër G, Bégin-Colin S and Delcroix P 2003 *Material Research in Atomic Scale by Mössbauer Spectroscopy* (*NATO Science Series II–Mathematics, Physics and Chemistry* vol 94) ed M Mashlan, M Miglierini and P Schaaf (Dordrecht: Kluwer) pp 11–20
[56] Froseth A G, Derlet P M and Van Swygenhoven H 2005 *Adv. Eng. Mater.* **7** 16–20
[57] Wu X L and Zhu Y T 2008 *Phys. Rev. Lett.* **101** 025503
[58] Zhu Y T and Liao X Z 2005 *Appl. Phys. Lett.* **86** 095701
[59] Cao A J and Wei Y G 2006 *Appl. Phys. Lett.* **89** 041919
[60] Huang J Y, Yu Y D, Wu Y K, Li D X and Ye H Q 1997 *Acta Mater.* **45** 113–24
[61] Wu X L, Liao X Z, Srinivasan S G, Zhou F, Lavernia E J, Valiev R Z and Zhu Y T 2008 *Phys. Rev. Lett.* **100** 095701
[62] Stappert S, Rellinghaus B, Acet M and Wassermann E F 2003 *Eur. Phys. J.* D **24** 351–4
[63] Rollmann G, Gruner M E, Hucht A, Meyer R, Entel P, Tiago M L and Chelikowsky J R 2007 *Phys. Rev. Lett.* **99** 083402
[64] Bove L E, Petrillo C, Sacchetti F and Mazzone G 2000 *Phys. Rev.* B **61** 9457–66